JOINT EUROPEAN TORUS JET

JET–P(87)57

P.C. Stangeby, J.A. Tagle, S.K. Erents
and C Lowry

Measurements of the Cross-field Diffusion Coefficient $D_\perp$ in the Edge Plasma of JET

Measurements of the Cross-field Diffusion Coefficient $D_\perp$ in the Edge Plasma of JET

P.C. Stangeby[1], J.A. Tagle[2], S.K. Erents[3]
and C Lowry[4]

JET-Joint Undertaking, Culham Science Centre, OX14 3DB, Abingdon, UK

[1]Institute for Aerospace Studies, University of Toronto, Ontario, Canada
[2]JET-Joint Undertaking, Culham Science Centre, OX14 3DB, Abingdon, UK
[3]Culham Laboratory, Abingdon, Oxon, UK
[4]Imperial College of Science and Technology, London, UK

Preprint of Paper to be submitted for publication in
Plasma Physics and Controlled Fusion

Abstract

In relating the density scrape-off layer thickness λ_n to $D_\perp$, account is taken of two aspects of the JET configuration: (a) the poloidally-varying cross-section of plasma flux tubes in the scrape-off layer, and (b) the different limiter configurations - discrete/continuous.

It is found that when poloidal variations are dominated by configuration, rather than fluid flow effects, the density scrape-off length at the outside mid-plane, λ_n ($\theta = 0$) is given by the theoretical relation

$$\frac{c_s \lambda_n^2(0)}{f D_\perp \pi (R_m + a)} = \begin{cases} q_s(0) \text{ for } q_s(0) > q_s^*(0) \\ q_s^*(0) \text{ for } q_s(0) < q_s^*(0) \end{cases}$$

for the case of N equally-spaced, rail limiters each of plasma-wetted height h_w located symmetrically around the outside mid-plane. f is a shape factor of order 0.5 which varies slightly with plasma shape and the other symbols have their usual meaning. q_s is the normalized pitch of the field at the limiter, rather than a safety factor: $q_s(0) \equiv r(0)\, B_\phi(0)/R(0)B_\theta(0)$, $q_s^*(0) \equiv 2\pi a/h_w N$.

For $q_s(0) \geq q_s^*(0)$ all field lines passing through the outside mid-plane strike a limiter, hence the set of discrete limiters acts as a complete toroidal (belt) limiter. The first expression also applies to the latter type of limiter. For $q_s(0) < q_s^*(0)$, λ_n is predicted to be independent of q and dependent on N.

Edge measurements of $\lambda_n(0)$ in JET made by Langmuir Probes and limiter-viewing cameras are used to deduce edge values of $D_\perp$ for ohmic discharges, over a range of conditions, I_p = 1-5 MA, $\bar{n}_e$ = 0.7 - 6 x 10^{19} m^{-3}. Generally the values are found to be close to $D_\perp = 10^{19}/\bar{n}_e$ m^2/s, that is, Intor-Alcator scaling.

1. Introduction

The cross-field diffusion coefficient $D_\perp$ in the plasma edge can, in principle, be evaluated from measurement of the density scrape-off length, λ_n. One has approximately that[1]

$$\lambda_n = (LD_\perp/c_s)^{\frac{1}{2}} \qquad (1)$$

where L is the connection length (limiter spacing of 2L along $\bar{B}$) and c_s is the ion sound speed. It will be shown here that in a non-circular tokamak such as JET employing discrete limiters, the usual expression for L

$$L \simeq \pi R_m q_s \qquad (2)$$

can be significantly in error (R_m is the plasma major radius, q_s is the value of the safety factor on the Last Closed Flux Surface, LCFS). As a result, uncertainty is introduced in the inference of $D_\perp$ from λ_n.

The value of $D_\perp$ is of interest in several contexts:

(a) In many circumstances it is possible to describe the complete plasma profile n(r) by a model which assumes diffusion plus a small inward pinch velocity v_{in}, typically

$$\Gamma(r) = - D_\perp \frac{dn}{dr} + v_{in}$$

with $v_{in} = - 2D_\perp \, r/a^2$

where Γ = plasma flux density cross-field
a = plasma minor radius

This gives the result for an edge-fuelled plasma:

$$n(r) = \frac{\phi_H{}^0}{D_\perp} (\lambda_H{}^{iz} + \lambda_n) \exp \left[1 - (r/a)^2\right] \qquad (3)$$

where $\phi_H{}^0$ = neutral hydrogen fuelling rate at the edge (H/sec)

$\lambda_H{}^{iz}$ = average neutral hydrogen penetration, typically ~ 0.1 m.

Equation (3) is strictly only valid if $D_\perp$ is not a function of r. If $D_\perp(r)$ then eqn. (3) is still approximately correct, provided the value of $D_\perp$ near the edge ($a - \lambda_{iz}{}^H < r < a$) is employed. That is, the

entire density profile is dominated by the edge value of $D_\perp$.

(b) The radial profile of impurity ions is also often described[2] by the equivalent of eqn. (3) with ϕ_H^0 replaced by ϕ_{imp}^0, the impurity influx form the edge due, e.g., to sputtering of limiters, and λ_H^{iz} is replaced by λ_{imp}^{iz}, of order 1 cm. Thus the impurity levels throughout, the plasma are largely controlled by edge parameters, including $D_\perp$ in this anomalous (not neo-classical) transport model.

(c) The achievement of high performance modes of tokamak operation such as the H-mode, characterized by improved energy confinement, may be dependent on reductions of $D_\perp$ near the edge[3].

(d) Planning for the introduction of new components into the scrape-off layer, SOL, e.g. RF Antennae, Pumped Limiters etc. requires knowledge of $D_\perp$ since the additional components change L and thus the value of λ_n in their absence, effecting the thermal and particle loading.

It is therefore of interest to measure $D_\perp$ over a range of plasma conditions - plasma current I_p, plasma density $\bar{n}$, magnetic field B_ϕ. It is also of interest to measure $D_\perp$ near the plasma edge and to establish whether it differs appreciably from central plasma values.

2. Connection Lengths

2.1 Toroidal Belt Limiter

Geometrical quantities are defined in Fig. 1. For the case of a complete toroidal belt limiter located at the outside mid-plane, $\theta = 0$, the flow symmetry point is at $\theta = \pi$ and the connection length is

$$L = \int_{\theta=0}^{\pi} d\ell = \int_{o}^{\pi} \frac{B(\theta)}{B_p(\theta)}\, r(\theta)\, d\theta \qquad (4)$$

where $B_p(\theta)$ = poloidal field on the LCFS
$B(\theta)$ = total field on the LCFS.

One has the actual q, q_ψ, on the LCFS

$$q_{\psi s} = \frac{1}{2\pi} \int_{o}^{2\pi} B_\phi(\theta)\, \frac{r(\theta)d\theta}{R(\theta)\, B_p(\theta)} \qquad (5)$$

and so approximately

$$L \approx \pi R_m q_{\phi s}. \tag{6}$$

One may note that q_ϕ is generally bigger than q_{cy}:

$$q_{cy} \approx \frac{2\pi a^2 \kappa B_{\phi o}}{R_m \mu_o I} \tag{7}$$

where $\kappa \equiv b/a \equiv$ plasma elongation.

2.2 Discrete Limiters on JET

Until 1987 JET had up to 8 discrete limiters with dimension (poloidal height) h = 0.8 m and (toroidal) width w = 0.4 m located on the outside midplane at $R_L = R(0) = 4.16$ m.

Consider a set of N discrete limiters located symmetrically (toroidal direction) around the outside mid-plane, each of poloidal height h, see Fig. 2. There will be next-neighbour shadowing of limiters when

$$\frac{2\pi(R_m + a)}{Nh} < \frac{B_\phi(0)}{B_p(0)}. \tag{8}$$

(The toroidal width of the limiters can be neglected when $w << h$ $\frac{B_\phi(0)}{B_p(0)}$, as is general). In this situation the set of discrete limiters will act, in effect, as a continuous toroidal limiter.

We may define a normalized field-line angle at the outside midplane by $q_s(0)$:

$$q_s(0) \equiv \frac{r(0)\, B_\phi(0)}{R(0)\, B_p(0)} \tag{9}$$

where $R(0) = R_m + a$
$r(0) = a$.

It may be noted that $q_s(0)$ has the form, although not the function, of a safety factor.

Then criterion (8) can be re-written as

$$q_s(0) > q_s^*(0) \tag{10}$$

where $q_s^*(0) \equiv \frac{2\pi a}{hN}$ (11)

is the critical value of $q_s(0)$ for the discrete limiters to act as a continuous toroidal one.

For illustration consider the example of JET discharge 3050 at t = 6 sec (R_m = 2.98 m, $B_{\phi m}$ = 3.44 T, I_p = 3.6 MA, κ = 1.445, $q_{\phi s}$ = 4.505). Table 1 gives values for $B_p(\theta)$ etc. on the LCFS. One thus finds that for this case $q_s(0)$ = 1.23 i.e. much smaller than $q_{\phi s}$, which is, in fact, a general result.

The geometrical height of a discrete JET limiter is 0.8 m; however, due to the poloidal curvature of the plasma and the fact that the limiters are vertically straight, the plasma-wetted height h_w is less than 0.8 m. In some circumstances the information is available from the limiter-viewing camera on the height h_w of the wetted area. Otherwise h_w can be calculated from the measured value of $\lambda_n(0)$ together with information on the plasma curvature at θ = 0. The latter is $\approx a\kappa$, typically, on JET giving $h_w \simeq 2\left(2a\kappa\lambda_n(0)\right)^{\frac{1}{2}}$. For purposes of illustration we take this to be 0.4 m in the following. It should, however, be calculated individually for each discharge condition.

For the case of Table 1 we thus find that for $N \geq 2\pi a/\left(h_w q_s(0)\right) \simeq 14$ the discrete limiters will act as a toroidal one. For $N < 14$, there will be field lines which do not strike a limiter on their first pass through the outside mid-plane, but will require additional toroidal/poloidal transits. For rational values of $q_{\phi s}$ there will be some field lines which never strike a limiter. Therefore, a wide range of connection lengths will exist for different flux tubes in the same SOL. In such a situation one might expect to observe substantial "structure" in the SOL. For example, for some values of $q_{\phi s}$ an edge probe would be on a field line for which L = ∞ but with a small change in q, L would drop to $\simeq \pi Rq$. This might be expected to result in sharp changes in values of density etc. measured by the probe. Although JET has been operated with N = 4 and 8, such structure has not been observed in probe characteristics.

In Ref. 4 it is suggested that q-related structure could be smoothed out by (poloidal) cross-field transport between adjacent flux tubes, some of which terminate on a limiter at the next mid-plane pass and some which miss. Poloidal EXB drift velocities have been inferred from probe measurements on JET[4] of a magnitude approaching 10^3 m/s. The poloidal distance which must be traversed in order to "short" out very long connection lengths is a fraction of h. This must be achieved in the parallel transport time $\tau_\parallel \simeq L/c_s \simeq \pi Rq/c_s \simeq 1$ msec.

A value of $V_{pol} \simeq 10^3$ m/s would be adequate to achieve such a shorting effect, although if it were poloidally constant only a twist effect would result, rather than a smoothing one.

For simplicity, we proceed on the assumption that all parallel-field plasma flow in the SOL terminates at the outside mid-plane for N "large enough". (It turns out, however, that this assumption does not effect the final result see below). Thus the collection of discrete limiters continues to act as a toroidal limiter and $L \simeq \pi R q_s$. The question of how small a value of N still satisfies this assumption requires more information on poloidal transport.

For N sufficiently small one could approximate the collection of discrete limiters as a partial poloidal limiter. Averaging over the resonances which occur because of the periodicity of both the magnetic and limiter structures, one has that the fraction of a full poloidal ring spanned is

$$g = Nh_w/2\pi a \tag{12}$$

and one could take the connection length to be approximately

$$L = \pi R/g \tag{13}$$

$$= 2\pi^2 aR/Nh_w. \tag{14}$$

If we assume that N = 4 acts as a toroidal limiter for the case of Table 1, (while for $N < 4$ eqn. (13) holds), this defines an effective limiter height h_{eff} from eqn. (10) namely $h_{eff} = 1.48$ m.

In Appendix I a theoretical relation is found between $\lambda_n(0)$ and $D_\perp$ allowing for a non-circular plasma and limiters which are either continuous (toroidal belt limiter) or a set of discrete rails. It is found in agreement with simple modelling that $\lambda \propto D_\perp^{\frac{1}{2}}$, however, the constant of proportionality is smaller. For a set of discrete limiters a regime is identified where λ_n is independant of q (neglecting resonances between the periodicity of the limiter structure and the magnetic field structure). The possibility that non-geometrical factors play a role in the relation between λ_n and $D_\perp$ is examined in Appendix II; it is concluded that such effects do not appear to be strong for the JET cases considered.

3. Examples of $D_\perp$ from λ_n

We consider a number of examples of JET discharges, and assume that $n(\theta)$ = constant and $\Lambda(\theta) = 1$. From eqns. (I.8), (I.12) and (I.14) we have

$$\lambda_n^2(0) = \begin{cases} D_\perp f\pi (R_m + a)\, q_s(0)/c_s & \text{for } q_s(0) > q_s^*(0) \\ D_\perp f\pi (R_m + a)\, q_s^*(0)/c_s & \text{for } q_s(0) < q_s^*(0) \end{cases} \qquad (15)$$

The f factors are calculated in Table 2 from computed magnetic profiles during the current flat-top; ohmic discharges only.

Only top probe data were available for discharge 3752. For this discharge $\lambda_n(0)$ was inferred from the measured $\lambda_n(80°) = 9.2$ cm using $\Delta r(80°)/\Delta r(0) = 2.7$ for this discharge, hence $\lambda_n(0) = 3.4$ cm. For the other cases the values of $\lambda_n(0)$ were taken from the mid-plane probes.

It may be noted that the values of $D_\perp$ inferred using equation (15) are 2 - 3 times larger than deduced using the simpler formulation employed in reference 4.

Rather than calculate $q_s(0)$ for each discharge, the simple straight line fits to q_{cyl} vs $q_s(0)$ and q_ϕ vs $q_s(0)$, Fig. 7, were used. Figure 8 gives values of $D_\perp$ obtained using eqn. (15) for a number of ohmic JET discharges, displayed as a function of $\bar{n}_e$ and I_p. The discharges examined were restricted to ones defined by the outer limiters (X-point and inner wall discharges were excluded).

The quality of probe data for the low current discharges is not good which may account for the large scatter in $D_\perp$ values for low $\bar{n}_e$ and low I_p.

The limiter was viewed with a CCD camera employing a filter for Hα light. The footprints provide a measure of λ_Γ. Since the camera technique does not provide a measure of λ_T, for simplicity λ_Γ was used in eqn. (15) in place of λ_n. The i.r. results in Fig. (8) are for four individual discharges followed in time as $\bar{n}_e$ varied.

These edge values of $D_\perp$ may be compared with a number of measurements made by other techniques on JET - for the main plasma:

(a) A spectroscopic measurement[12] of $D_\perp = 1$ m^2/s was made in an ohmic discharge, $I_p = 2.8$ MA, $B_T = 3.4$T, $\bar{n}_e = 2 \times 10^{19}$ m^{-3}, from the temporal decay of a Ni XXVI (central plasma) line after a metal injection.

(b) A reflectometer measurement[13] of $D_\perp = 0.8\ m^2/s$ was made for an ohmic discharge, $I_p = 3MA$, $B_T = 2.9T$, $\bar{n}_e = 2.3 \times 10^{19}\ m^{-3}$ based on the rate of radial propagation of density pulses associated with sawtooth oscillations.

(c) Values of $D_\perp(r)$ were obtained[14] from the density build-up induced by low level ICRF heating (2 MW), in a $I_p = 2MA$, $B_T = 2.3T$, $\bar{n}_e = 2 \times 10^{19}\ m^{-3}$ plasma, giving

$$D_\perp(r) = 0.33\ (1 + 2r/a^2)$$

valid for $0 \leq 0.8$, which gives $\bar{D}_\perp = 0.7\ m^2/s$.

For comparison purposes these values of $D_\perp$ are also plotted in Fig. 8. It would appear that for JET ohmic discharges the edge values of $D_\perp$ do not differ significantly from the average values, at least on the basis of this limited comparison.

Aside from the $I_p = 1MA$ data, which was characterised by poor probe signal/noise and wide scatter in $D_\perp$, most of the values of $D_\perp$ approximate to INTOR-ALCATOR scaling $\approx 10^{19}\ \bar{n}_e^{-1}$.

Since operationally, $\bar{n}_e$ and I_p tend to be coupled, the results of Fig. 8 can also be viewed as evidence for a $D_\perp(I_p)$ dependance. Finally, probe measurements[4] of edge plasma temperature $T_e(a)$ on JET show that $T_e(a)$ decreases with increasing $\bar{n}_e$; thus the results of Fig. 8 can also be viewed as evidence of Bohm-like diffusion.

4. Conclusion

A theory is presented for inferring values of the cross-field diffusion coefficient $D_\perp$ in the plasma edge from measurements of the scrape-off layer thickness. The theory allows for discrete limiter geometry and non-circular plasma cross-sections.

Applied to data from ohmic JET discharges defined by 4 or 8 outer limiters, the model gives values of $D_\perp$ which are close to $D_\perp = 10^{19}\bar{n}_e^{-1}$ i.e. Intor-Alcator scaling. These edge values are also close to the measurement of central $D_\perp$ made on JET.

Acknowledgements

The authors wish to thank S.A. Cohen, G. Maddison and C.S. Pitcher for their helpful comments. P.C. Stangeby acknowledges support by the Canadian Fusion Fuels Technology Project.

Table 1 SHOT # 3050 t = 6 sec R_m = 2.98 m $B_{\phi m}$ = 3.44 T

POINTS ON LAST CLOSED FLUX SURFACE ϕ_s

(R, Z) = co-ordinates of points on LCFS

R [m]	Z [m]	B_p [T]	θ [degrees]	r [m]	rΔθ [m]	$\frac{r\Delta\theta}{B_p R^2}$	Δφ [deg]	φ [deg]	RΔφ [m]	Σ rΔθ [m]	ΣRΔφ [m]
4.110	0	0.56	0	1.13				0	0	0	0
4.018	0.573	0.56	29°	1.18	0.60	0.067	39°	39°	2.73	0.60	2.73
3.839	0.986	0.49	49°	1.31	0.46	0.064	38°	77°	2.55	1.06	5.28
3.356	1.506	0.37	76°	1.55	0.73	0.175	103°	180°	6.03	1.79	11.31
2.894	1.679	0.31	93°	1.68	0.50	0.193	113°	293°	6.11	2.29	17.42
2.512	1.606	0.30	106°	1.67	0.39	0.206	121°	414°	5.30	2.68	22.7
2.171	1.301	0.47	122°	1.53	0.43	0.194	114°	528°	4.32	3.11	27.0
1.93	0.848	0.63	141°	1.35	0.45	0.192	113°	641°	3.81	3.56	30.9
1.813	0.374	0.80	162°	1.21	0.44	0.167	98°	739°	3.10	4.0	34.0
1.786	0	0.82	180°	1.19	0.37	0.142	83°	822°	2.60	4.37	36.6

$$\sum \frac{r\Delta\theta}{B_p R^2} = 1.40 \quad (0 \leq \theta \leq 180°)$$

$$\therefore 2\,\frac{R_o\, B_{\phi m} \sum \frac{r\Delta\theta}{B_p R^2}}{2\pi} = 4.57$$

compare q_s = 4.505
from full magnetic code analysis.

Table 2 $D_\perp$ from λ_n

JET Discharge	3752	7108	7126	8928-36
I_p [MA]	1.1	3	2	3
$\bar{n}^p$ [$10^{19} m^{-3}$]	1.0	2.0	1.7	2.2
$B_{\phi m}$ [T]	3.4	3.5	3.5	2.9
N	4	8	8	8
κ	1.40	1.45	1.45	1.45
$\lambda_n(0)$ [cm]	3.4	1.0	1.2	1.0
h_w [m]	0.67	0.37	0.41	0.37
$q_s^*(0)$	2.7	2.6	2.3	2.6
$q_s(0)$	3.6	1.7	2.1	1.4
T(a) [eV]	17	100	80	40
f	0.47	0.54	0.54	0.54
$D_\perp$ [m^2/s]	2.1	0.56	0.79	0.35

References

1. K. Uehara et al, Plasma Physics 21, (1979), 89.

2. W. Engelhardt et al, Plasma Physics and Controlled Fusion, 28, (1986) 1401.

3. M. Watkins, private communication and S A Cohen et al, Plasma Physics and Controlled Fusion, in press.

4. S.K. Erents et al, Nucl. Fusion, 1986.

5. P.C. Stangeby, Phys Fluids 28 (1985) 644.

6. P.C. Stangeby, J. Nucl. Mater. 121 (1984) 55.

7. G.M. McCracken and P.C. Stangeby, Plasma Phys. and Controlled Fusion 27 (1985) 1411.

8. P.C. Stangeby, J. Nucl. Mater. 145-147 (1987) 105.

9. B. La Bombard and B. Lipschultz, Nucl. Fusion, 27 (1987) 81.

10. U. Samm et al, J. Nucl. Mater, 145+147, (1987), 206.

11. J. Lingertadt, et al, Proc. 11th IAEA Int. Conf. on Plasma Physics and Controlled Fusion, Kyoto, 13-20 Nov 1986.

12. K. Behringer et al, Proc. 11th IAEA Int. Conf. on Plasma Physics and Controlled Fusion, Kyoto, 13-20 November 1986.

13. A. Hubbard, D Ward and T E Stringer, Proc. 13th European Conf. on Controlled Fusion and Plasma Physics, Schliersee, 1986, I, 232.

14. A. Cheetham et al, Proc. 13th European Conf. on Controlled Fusion and Plasma Physics, Schliersee, 1986, I, 240.

Appendix I. Expressions for $\lambda_n(D_\perp)$

I.1 Toroidal Belt Limiter

For non-circular JET discharges the radial separation between flux surfaces, $\Delta r(\theta)$, is dependent on poloidal angle with separation being greater at the top/bottom of the torus than the mid-planes. ($\Delta r(\theta)$ also varies somewhat with minor radius, but this effect is not significant over the SOL thickness). This variation is plotted in Fig. 3 for the example of Table 1. Clearly this effect by itself will cause λ_n to strongly vary poloidally. We assume here that in the absence of any other causes of poloidal variations (such as poloidal variation in $D_\perp$, $D_\perp(\Theta)$) that

$$\lambda_n(\theta)/\lambda_n(0) = \Delta r(\theta)/\Delta r(0). \qquad (I.1)$$

It is also evident from Fig. 3 that the poloidal width, $w(\theta)$, of any flux tube is also dependent on θ. In addition, the cross- sectional area of the flux tube also varies with θ, $A(\theta)$; Fig. 3.

Consider an elemental area of plasma surface δA, (not to be confused with $A(\theta)$) its normal parallel to the (small) radial direction, and aligned with $\vec{B}$, see Fig. 4.

$$\delta A = \frac{B_\phi(\theta)}{B_p(\theta)}\, w(\theta)\, r(\theta)\, d\theta \qquad (I.2)$$

For a full toroidal limiter at $\theta = 0$ one has from the balance between particle flux cross-field into the flux tube and parallel flow at the sound speed into the limiter:

$$\int_{r=0}^{a_w} \frac{B_\phi(0)}{B(0)}\, \Gamma\,(\theta = 0,\ r)\, w(0)\, dr = \int_{\theta=0}^{\pi} D_\perp \frac{dn}{dr}\, \delta A$$

where i) $\frac{B_\phi(0)}{B(0)}\, w(0)$ is the projected height of the flux tube perpendicular to $\bar{B}$.

ii) $\Gamma\,(\theta = 0,\ r)$ the flux density at $\theta = 0$ is assumed to vary exponentially with a characteristic length $\lambda_n(0)$ (rather than the more accurate $\left[(\lambda_n(0)^{-1} + (2\lambda_T(0)^{-1}\right]^{-1}$) i.e. $\Gamma(\theta = 0,\ r) = n\,(0)\, c_s \exp\left[-r/\lambda_n(0)\right]$.

iii) a_w = distance to the wall. It is assumed that $a_w >> \lambda_n(0)$.

iv) The SOL influx term, RHS, assumes that ionisation within the SOL is a negligible source.

The foregoing leads to

$$\left[n(o)c_s \frac{B_\phi(0)}{B(0)}\right] \lambda_n(0)\ w(0) = \int_{\theta=0}^{\pi} D_\perp \frac{dn}{dr}\ \delta A \qquad (I.3)$$

One may allow for possible variation $\lambda_n(\theta)$ due to factors other than field line compression, such as fluid flow effects, which generalizes eqn. (I.1) to:

$$\frac{\lambda_n(\theta)}{\lambda_n(0)} = \frac{\Delta r(\theta)}{\Delta r(0)} \Lambda\ (\theta). \qquad (I.4)$$

Where $\Lambda(\theta)$ allows for such additional effects on λ_n.

Assuming that $D_\perp$ does not change as the separatrix is crossed radially, and allowing for the possibility that density varies poloidally:

$$\frac{dn}{dr} = \frac{n(\theta)}{\lambda_n(\theta)} \qquad (I.5)$$

plus the relations for $\Delta r(\theta)$ and $w(\theta)$ which may be shown to be:

$$\frac{\Delta r(\theta)}{\Delta r(0)} = \frac{R(0)\ B_p(0)}{R(\theta)\ B_p(\theta)} \qquad (I.6)$$

$$\frac{w(\theta)}{w(0)} = \frac{R^2(\theta)\ B_p(\theta)}{R^2(0)\ B_p(0)} \qquad (I.7)$$

one obtains

$$\lambda_n^2(0) = \frac{D_\perp\ r(0)\ B(0)}{c_s\ B_p(0)} \int_o^{\pi} \frac{n(\theta)}{n(0)} \frac{1}{\Lambda(\theta)} \frac{w(\theta)}{w(0)} \frac{r(\theta)}{r(0)}\ d\theta \qquad (I.8)$$

where $D_\perp$ is constant, or alternatively may be considered to be the poloidally-weighted average according to the integral in eqn. (I.8). The fact that $B_\phi(\theta)\ R(\theta)$ = constant has also been used.

One may consider the example of a circular discharge:

$$R(\theta) = R_m + a \cos \theta$$

$\kappa = 1$

$r(\theta) = a$

$$B_\phi(\theta)/B_p(\theta) = \text{const.} \qquad \text{(I.9)}$$

Also assume $n(\theta)$ = constant and $\Lambda(\theta) = 1$, thus $\lambda_n(\theta)$ = constant. One obtains

$$\lambda_n(0) = (D_\perp L/c_s)^{\frac{1}{2}}$$

$$\text{with} \quad L \equiv \pi R_m \, q_{cy} \left(\frac{B(0)}{B_\phi(0)}\right) \left(\frac{R_m}{R_m + a}\right)^2 \qquad \text{(I.10)}$$

$$\text{where} \quad q_{cy} = \frac{a\,(R_m + a)}{R_m^{\,2}} \frac{B_\phi(0)}{B_p(0)} \qquad \text{(I.11)}$$

from eqn. (7).

Example: $R_m = 3$m, $a = 1$ m,
$B_{\phi m} = 3.4$T, $\therefore B_\phi(0) = 3.4 \times 0.75 = 2.55$ T,
$I_p = 3$ MA $\therefore B_p(0) \approx \mu_o I/2\pi a = 0.6$ T $\therefore B = 2.62$ T
and $L = 0.58\ \pi R_m\, q_{cy}$, which is close to the simple estimate, eqn (2).

Turning to the case of non-circular plasmas with a full toroidal, mid-plane limiter, we initially take $n(\theta)$ = const. and $\Lambda(\theta) = 1$, and define

$$f \equiv \pi^{-1} \int_0^\pi \frac{w(\theta)}{w(o)} \frac{r(\theta)}{r(o)}\, d\theta. \qquad \text{(I.12)}$$

The value of f for the specific example of Table 1 is found to be 0.54. Thus for this specific case

$$\lambda_n^2(0) = \frac{0.54\ D_\perp\ \pi\ r(0)\ B(0)}{c_s\ B_p(0)} \qquad \text{(I.13)}$$

$$\simeq 0.54\ D_\perp\ \pi\ (R_m + a)\ q_s(0)/c_s. \qquad \text{(I.14)}$$

Strictly, each discharge condition should be separately analysed to evaluate the integral in eqn. (I.8) for the actual LCFS shape, also using the particular values of $r(0)$, $B(0)$ and $B_p(0)$. It turns out, however, that the integral differs little between discharges; see Table 2. One can then generalize by using q_ψ to replace the

parameters in eqn. (I.13). For the example of Table 1 it is found that

$$q_\psi = \frac{3.63\ r(0)\ B_\phi(0)}{(R_m + a)\ B_p(0)} \cdot \tag{I.15}$$

Assuming that $B_\phi(0) \simeq B(0)$ one then has the generalization that

$$\lambda_n^2(0) = 0.14\ D_\perp \pi\ (R_m + a)\ q_\psi / c_s. \tag{I.16}$$

One may note that the effective connection length L_{eff}

$$L_{eff} = 0.14\ \pi\ (R_m + a)\ q_\psi \tag{I.17}$$

is substantially smaller than the simple value, eqn. (6). In the case of Table 1, $L_{eff}/L = 0.14\ (R_m + a)/R_m = 0.19$. Accordingly, the value of $D_\perp$ inferred from measured values of $\lambda_n(0)$ is underestimated by a factor of ~ 5, for this case, using the simple relation.

I.2 Discrete Limiters

For $N \geq N_{max} \equiv 2\pi a/h_w q_s(0)$ the discrete limiters act as a continuous toroidal limiter and the result of eqn. (I.12) apply.

For $N_{max} > N > N_{min} \equiv 2\pi a/\left(h_{eff}\ q_s(0)\right)$ the discrete limiters act as a toroidal limiter so far as connection length is concerned. In calculating λ_n, however, one must allow for the fact that the flux tube terminating on the limiter receives (radial) cross-field influx from the main plasma over a larger plasma surface area than that of the flux tube. That is the $w(\theta)$ in eqn. (I.2) should be replaced by $w(\theta)\ h'/h_w$, see Fig. 1

$$\text{where } \frac{h'}{h_w} = \frac{B_p(0)}{B_\phi(0)} \frac{2\pi(R_m + a)}{Nh_w} \tag{I.18}$$

$$= \frac{2\pi a}{Nh_w q_s(0)} \cdot \tag{I.19}$$

This means that the expressions for $\lambda_n^2(0)$, eqns. (I.13) and (I.16) should be increased by the same factor h'/h_w. Introducing this to eqn. (I.13) we find

$$\lambda_n^2(0) \simeq \frac{(0.54)\ 2\pi^2\ a(R_m + a)D_\perp}{c_s\ Nh_w} \tag{I.20}$$

and thus one obtains the result that λ_n does not depend on q for this regime. That is for $q_s(0) \leq 2\pi a/Nh_w$ there is no q-dependence. For the example of a = 1.16 m, N = 8, h_w = 0.4 m this gives $q_s(0) \leq 2.28$. Making the assumption that $q_s(0) \propto q_{\psi s}$ one has from the example of Table 1, $q_{\psi s} \lesssim 8$.

It should not be thought that this transition to a q-independent value of λ_n at small q is a result of the assumption of poloidal transport between flux tubes. Consider the situation for no poloidal transport and the case of $q_s(0) = \frac{1}{2}\, q_s^*(0)$, say. For this q half the field lines do not strike a limiter on the first pass. Thus the most probable (although not average) trajectory is one of length 2π Rq (rather than π Rq which applies for $q \geq q^*$). Since 2π Rq = $2\pi R(\frac{1}{2}q^*) = \pi Rq^*$ one finds the result of a q-independent λ_n without invoking poloidal transport (at least for the most probable trajectory). This same conclusion can also be reached by considering the integral of eqn. (I.3) around the toroidal direction. That is, consider the entire scrape-off layer to be unravelled and flattened to a slab. The RHS would then give the total particle outflux of the plasma while the LHS would give the total flux to the limiters. This integration contributes the same factor to each side of the equation for a continuous (or effectively continuous collection of) limiter(s) but for $q_s(0) < 2\pi a/Nh_w$ the LHS only contributes for a fraction of the total toroidal circumference. This fraction is readily shown to be h_w/h', giving eqn. (I.20) again.

Appendix II. The Question of Poloidal Density Variations $n(\theta)$ and $\Lambda(\theta)$

One expects that the plasma density along the separatrix will vary for several reasons. In the simplest picture, that is constant-temperature inviscid flow along a duct of constant cross-sectional area, one assumes constant total pressure which implies that as the flow accelerates from stagnation at the symmetry point, its density drops by a factor 0.5 when the sound speed is reached (at the sheath edge). This density reduction can, however, be offset by a number of factors, and even reversed:

(a) Compression of the cross-sectional area of the plasma flux tube as it approaches the inside mid-plane in toroidal geometry, may be expected to cause a density increase.

(b) The plasma cools somewhat as it accelerates, and so the constant pressure assumption implies a density increase. This effect can be enormously enhanced by strong ionisation recycling near the limiter particularly if T_e is low (thus causing poor heat conduction along $\vec{B}$) and/or when flow friction is strong.

In short, the neglect of $n(\theta)$ and $\Lambda(\theta)$ variations is dependent on the SOL being "simple", defined[5] as one in which the limiter is the dominant energy and particle sink while cross-field transport from the main plasma is the dominant source. Local ionization of neutrals within the SOL, for example, must make a small contribution to particle balance, if the SOL is to be considered as simple; when local ionization is important λ_n increases[1,6]. Criteria have been derived[5], which use SOL values of n,T and L to indicate whether the SOL is simple or not[7,8]. For ohmic discharges on JET the SOL can thus be identified as being simple for much of the operating range, although the situation is marginal for the highest densities. Consider, for example, the question of ionization within the SOL. On JET the edge temperatures[4] are rather high compared to those measured in smaller tokamaks, with T_e at the LCFS ranging 30-200eV. In this situation direct ionization of the re-cycling D_2 becomes important (rather than dissociation into fast, Frank-Condon, atoms followed by atomic ionization). The penetration distance of a thermal D_2 molecule is only ~ 1 cm at the highest edge densities measured in JET, $\sim 10^{19}$ m^{-3} at the LCFS, and assuming the maximum ionization rate. This distance is to be compared with values[4] of $\lambda_n(0)$ which range down to about 1 cm at the highest I_p and $\bar{n}_e$, indicating that ionization within the SOL is not negligeable in this case.

One can also consider the experimental information on this question. Such data is very limited on JET. It consists of comparisons between Langmuir Probe data taken at the top of the torus, $\theta \simeq 80°$, and at the

outside mid-plane, $\theta \simeq 0$. Data of this nature is only available for the N = 8 limiter configuration. Figures 5 and 6 give an example of such data. The basic probe measurement is of I^+_{SAT}, the particle flux to the probe, Fig. 5. In this figure the spatial scale for the two probe positions has been corrected solely for the compression of the magnetic field lines between the top of the torus and the outside mid-plane. As can be seen this results in near coincidence of the two sets of data.

The primary quantity of interest, however, is the plasma number density n_e. The usual relation between n_e and I^+_{SAT} is

$$I^+_{SAT} = 0.5\ n_e\ c_s e \qquad \text{(II.1)}$$

where n_e is the density far from the probe (about one probe collection length, some metres for the JET top probe). The factor of 0.5 in eqn. (II.1) is due to the acceleration of the ions by the pre-sheath electric field created by insertion of the probe. It is due precisely to the acceleration effect described earlier which results in the plasma density just near the probe being approximately one half of the far field density. If a probe is immersed in a plasma which is already flowing toward it, then the factor of 0.5 is to be replaced by a larger value, approximately unity if the flow is sonic. Such is the case for the probes mounted near the outside mid-plane i.e. near the limiter. Thus the densities inferred from the I^+_{SAT} measurements are different by about 0.5 for the two probes on the same field line, Fig. 6. One may note, however, that the densities extrapolated to the LCFS (at $R_{pr} - R_{pl} = 0$) are less different. This experimental result is therefore not quite compatible with the simplest picture that $\lambda_n(\theta)$ and $n(\theta)$ are constant, but it is rather close. It is also worth noting that this experimental result implies a very much simpler SOL structure in JET than has been reported for poloidal limiter tokamaks such as Alcator[9]. In the latter device enormous poloidal variations have been observed with $\lambda_n(\theta)$ varying by 3 - 8 times with θ and the density (at the same minor radius) varying by even greater amounts. Smaller poloidal variations in $\lambda_n(\theta)$ and $n(\theta)$, of order 2, have been observed in the edge plasma of TEXTOR[10] operating with a set of movable rail limiters approximating to a poloidal limiter.

It must be acknowledged that the probe data for JET is very limited, consisting of only two locations (by contrast the Alcator data is based on 80 probe locations, poloidally distributed). It is quite possible that the apparent simplicity of the JET SOL is misleading and would be disproved by the use of data from additional probe positions. Assuming for the present, however, that the apparent simplicity is real, one may consider one obvious explanation: poloidal limiters interrupt communication between SOL flux tubes and thus facilitate the development of strong asymmetries. Consider, for example, the consequences of a poloidally varying $D_\perp(\theta)$. For a

poloidal limiter, particularly, at high q, each SOL flux bundle has a relatively small poloidal excursion, $\Delta\theta$, over its length. Thus since $\lambda_n \approx (D_\perp(\theta)L/c_s)^{\frac{1}{2}}$ one could have relatively strong variations in $\lambda_n(\theta)$. For a toroidal limiter, however, each flux bundle has a poloidal excursion $\Delta\theta = \pi$ from the stagnation point. While the source strength for particle influx, $D_\perp(\theta)\frac{dn}{dr}$, would then vary along the length of the flux tube, this does not cause λ_n to vary with θ (assuming pressure constancy along an (uninterrupted field line). Camera viewing of the limiters indicated next-neighbour shadowing of one limiter by another. The mid-plane probe was not located in such a shadow but had a clean "view" around the torus. On T10, long distance shadowing has been observed[11], that is, shadows resulting from multiple-toroidal-transits by flux tubes. If such long range shadowing occurred in JET it might be expected to be evidenced by abrupt changes in the probe signals as q varied slightly. Such structure has not been observed on JET and thus it is postutated, as discussed earlier, that poloidal cross-field mixing obliterates long range shadows on JET. Clearly for cases where multiple-toroidal transit shadowing persists, the extraction of $D_\perp$ values from measurements of λ_n is more complex than outlined here.

Finally, with regard to $\Lambda(\theta)$, Fig. 5 implies that $\Lambda(\theta) \simeq 1$ for this rather limited data set since $\lambda_n(o) \simeq \lambda_n(80°)$ when field-line compression is allowed for.

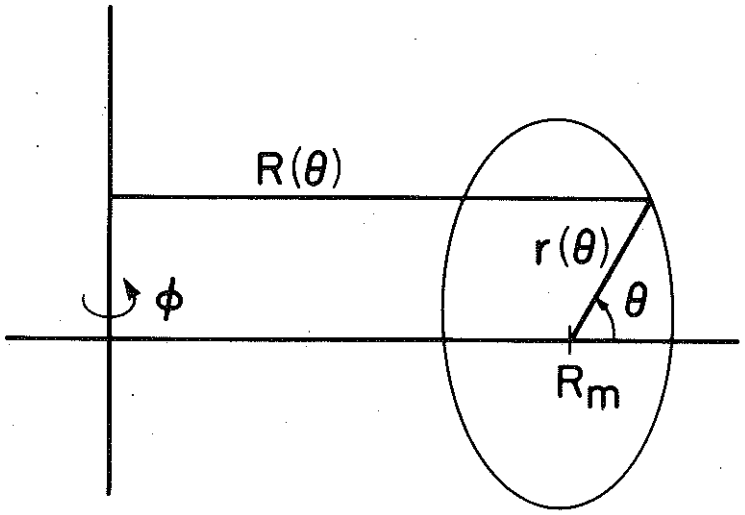

Fig. 1 Geometry of non-circular toroidal plasma.

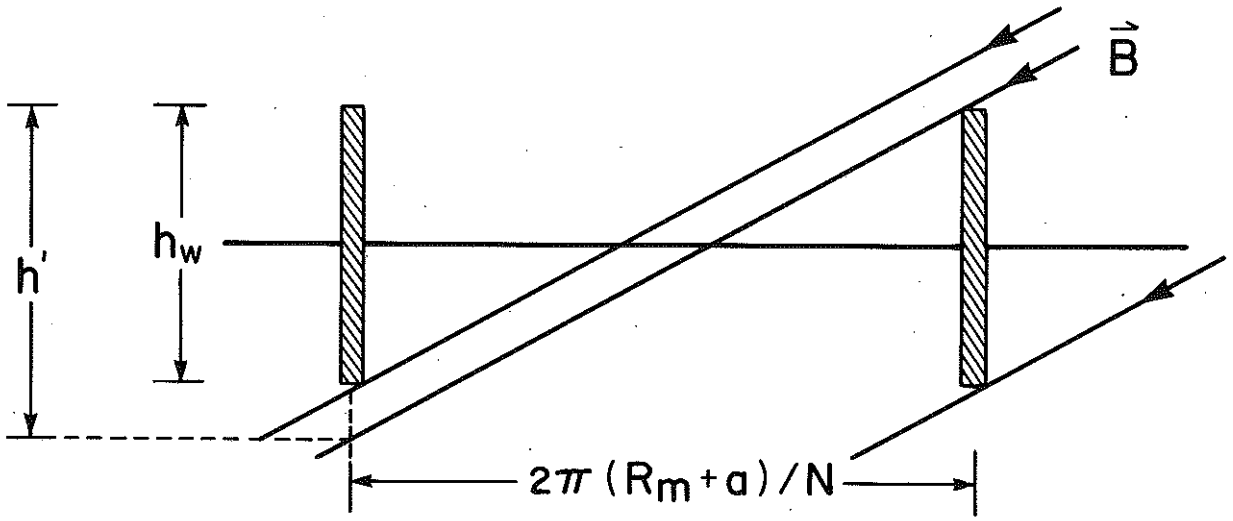

Fig. 2 Limiter spacing.

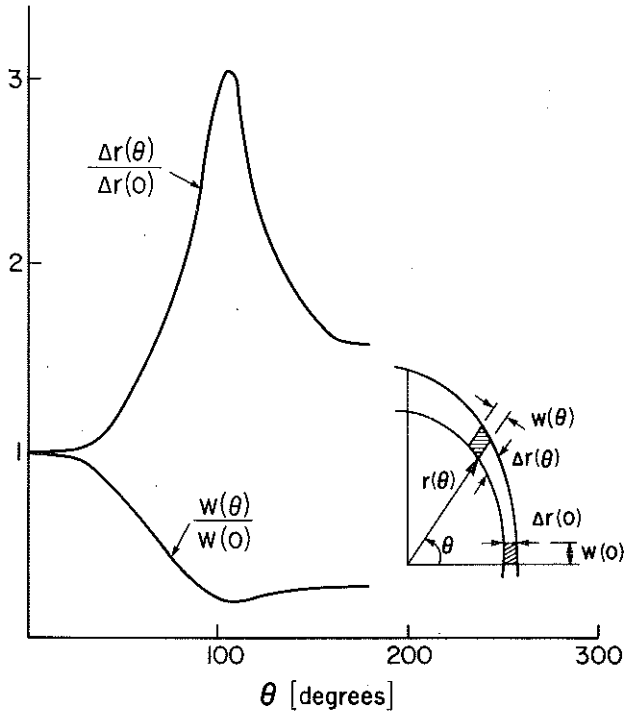

Fig. 3 Poloidal variation in flux tube cross-section for tube lying on Last Closed Flux Surface for JET discharge 3050 at $t=6$s

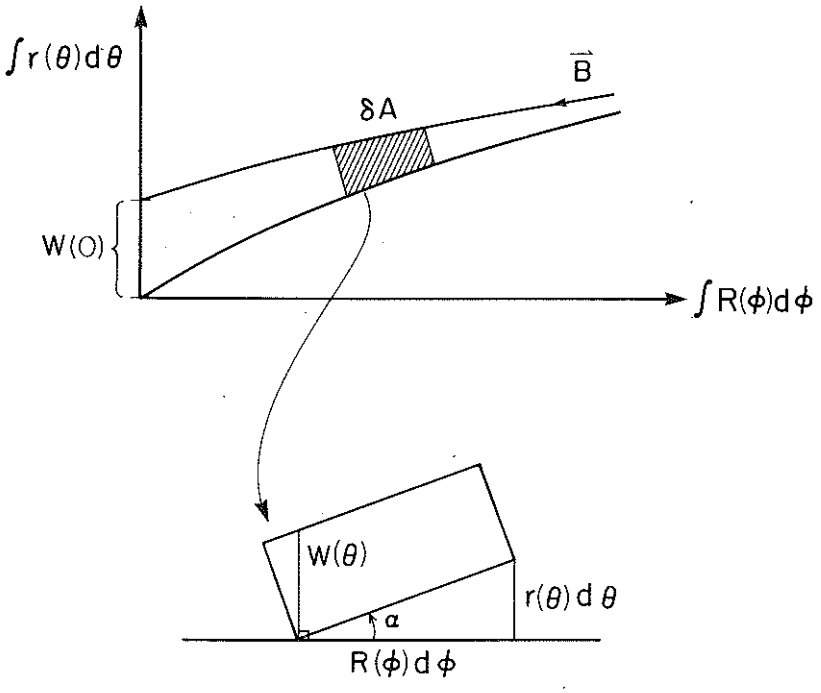

$$\tan \alpha = B_p(\theta)/B_\phi(\theta)$$

Fig. 4 Incremental area of flux tube surface.

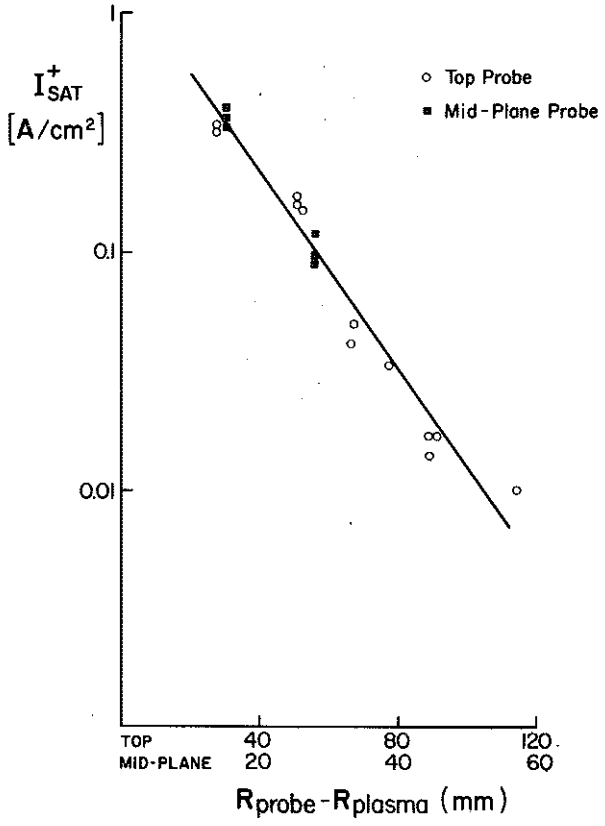

Fig. 5 Comparison of particle flux density measured by top Langmuir probe (0) and mid-plane probe (■). Discharges 8928, 8931-6. $I_p = 3$MA. $B_\phi = 2.8$T, $\bar{n}_e = 2.2\times10^{19}$m^{-3}. Indicated scrape-off length, λ, is for mid-plane.

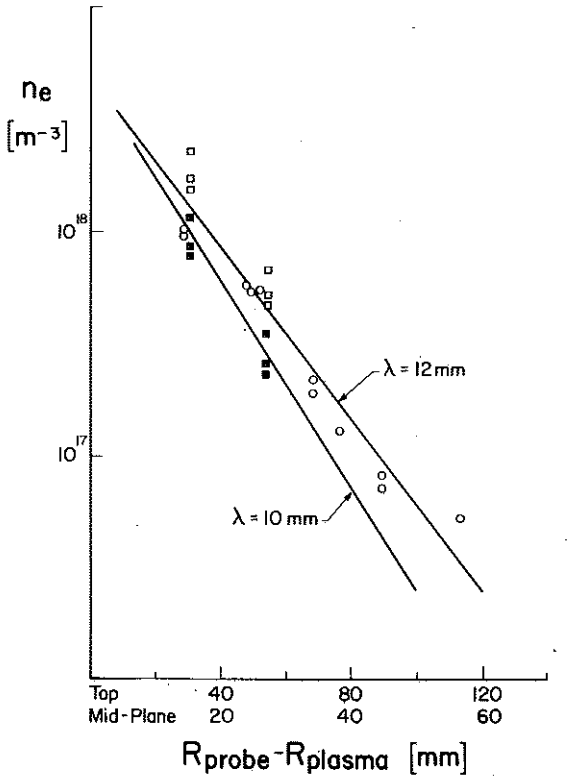

Fig. 6 Comparison of plasma density measured by top Langmuir probe (o) and mid-plane probe (□ using $I^+_{SAT} = n_e e c_s$). Discharges 8928, 8931-6, $I_p = 3$MA. $B_\phi = 2.8$T. $\bar{n}_e = 2.2\times10^{19}$m^{-3}. Indicated scrape-off lengths, λ, are for mid-plane.

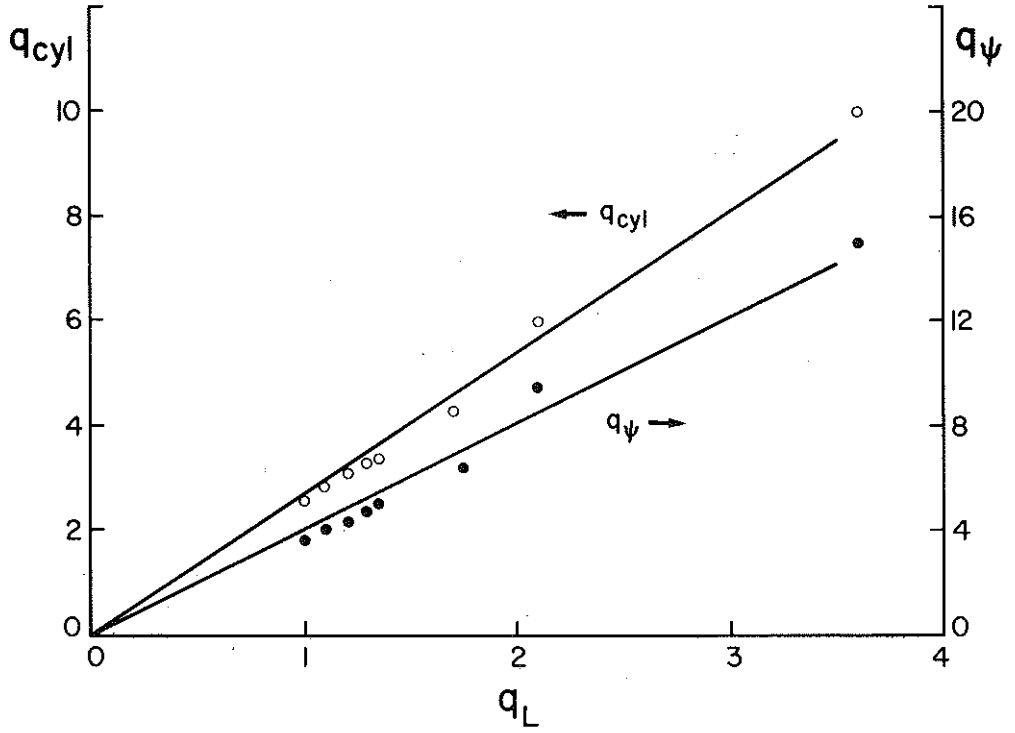

Fig. 7 Correlation between q_{cyl},q_ϕ and $q_s(0)$ for discharges with $\kappa \sim 1.5$.

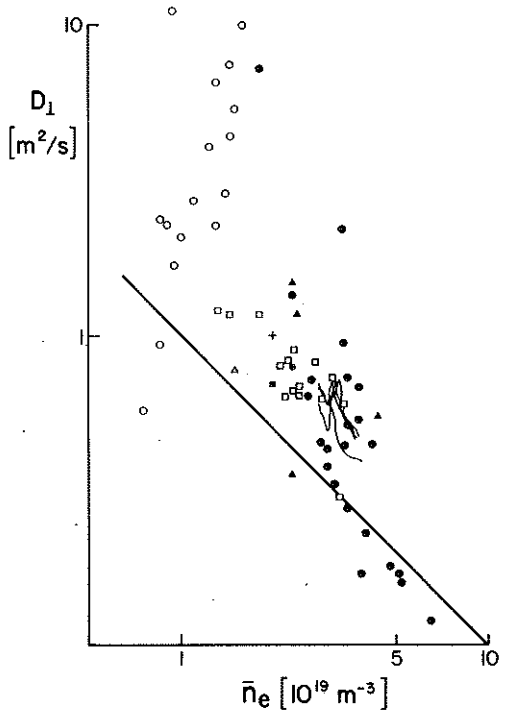

Fig. 8 Values of $D_\perp$ obtained from measurements of $\lambda_n(0)$. Probe data: 0 1MA, □2MA, ▲ 3MA, □4MA, ● 5MA. H_α camera viewing of limiter: wavy lines, four 5MA discharges. Solid line: $D_\perp = 10^{19}/\bar{n}_e$, INTOR-ALCATOR. Highest four densities points for He discharges, otherwise D_2. Central plasma measurements of $D_\perp$: + spectroscopic[12], ⊛ reflectometer[13], ⊞ density-rise experiment[14].